Spatially-targeted proteomics of the host-pathogen interface during staphylococcal abscess formation

Short Title: Proteomics of host-pathogen interface

Emma R. Guiberson[#1,2], Andy Weiss[#3], Daniel J. Ryan[1,2], Andrew J. Monteith[3], Kavya Sharman[1], Danielle B. Gutierrez[1], William J. Perry[1,2], Richard M. Caprioli[1,2,4,5,6], Eric P. Skaar*[3], Jeffrey M. Spraggins*[1,2,4]

[#]- authors contributed equally to this manuscript

*- Co-corresponding authors

Jeff.spraggins@vanderbilt.edu

Eric.p.skaar@vumc.edu

Affiliations:
(1) Mass Spectrometry Research Center, Vanderbilt University, Nashville, TN, USA
(2) Department of Chemistry, Vanderbilt University, Nashville, TN, USA
(3) Department of Pathology, Microbiology, and Immunology, Vanderbilt University, Nashville, TN, USA
(4) Department of Biochemistry, Vanderbilt University, Nashville, TN, USA
(5) Department of Medicine, Vanderbilt University, Nashville, TN, USA
(6) Department of Pharmacology, Vanderbilt University, Nashville, TN, USA

Abstract

Staphylococcus aureus is a common cause of invasive and life-threatening infections that are often multi-drug resistant. To develop novel treatment approaches, a detailed understanding of the complex host-pathogen interactions during infection is essential. This is particularly true for the molecular processes that govern the formation of tissue abscesses, as these heterogeneous structures are important contributors to staphylococcal pathogenicity. To fully characterize the developmental process leading to mature abscesses, temporal and spatial analytical approaches are required. Spatially targeted proteomic technologies, such as micro liquid extraction surface analysis, offer insight into complex biological systems including detection of bacterial proteins, and their abundance in the host environment. By analyzing the proteomic constituents of different abscess regions across the course of infection, we defined the immune response and bacterial contribution to abscess development through spatial and temporal proteomic assessment. The information gathered was mapped to biochemical pathways to characterize the metabolic processes and immune strategies employed by the host. These data provide insights into the physiological state of bacteria within abscesses and elucidate pathogenic processes at the host-pathogen interface.

Keywords: abscess formation/host-pathogen interface/microLESA/proteomics,/*Staphylococcus aureus*

Introduction

Staphylococcus aureus is one of the leading causes of bloodstream infections worldwide[1]. In the United States alone, this bacterium is responsible for more than 600,000 hospitalizations annually[2] and patients with *S. aureus* bacteremia have a 30-day mortality rate of 20%[3]. *S. aureus* bacteremia often spreads to other body sites leading to the formation of abscesses, most commonly affecting the liver, kidneys, brain, and heart tissues[4].

The formation of organ abscesses is a critical strategy to ensure *S. aureus* survival within the host[5]. Abscesses offer a temporary refuge for *S. aureus*, allowing the enclosed bacteria to resist the actions of the immune system, thereby securing persistence within host tissues[6,7]. In a murine model of systemic infection, the formation of soft tissue abscesses follows distinct phases (stages I-IV)[5], driven by the recruitment of immune cells (e.g. neutrophils) ~2 days post infection (dpi)[7], and the development of a bacterial nidus in the center of the abscess ~4-5 dpi (staphylococcal abscess colony, SAC)[7]. The developing SAC is surrounded by necrotic tissue, a fibrin pseudocapsule[7,8], and an outer microcolony-associated meshwork[6]. At the end of abscess development (~15-30 dpi), the persistent and increasingly larger lesions rupture and release bacteria that seed new abscesses or cause secondary infections[7].

Abscess formation requires the involvement of both host and bacterial factors. Several staphylococcal proteins, including both coagulases, Coa and vWbp, are essential for fibrin pseudocapsule formation and abscess development[9]. Additionally, a few other *S. aureus* proteins, associated with virulence, (e.g. Emp, Eap, Hla, IsdA, IsdB, SdrC, SrtA, Spa) have been found to be required for abscess formation[6-8,10,11]. The majority of these data describing bacterial contributions to abscess development were generated from histological stains or characterization of isogenic *S. aureus* mutants and their ability to persist within host tissues. However, unbiased studies that aim to assess the bacterial abscess proteome are sparse. This is similarly true for proteinaceous host factors in proximity to the abscess. While it is established that specific cell types (e.g. fibroblasts and neutrophils[12]) or immune proteins (e.g. the metal scavenging protein

calprotectin[13]) play essential roles during the immune response to *S. aureus*, we lack a detailed understanding of specific cellular processes involved in the host response to tissue colonization by *S. aureus*. Although a previous study from our laboratory addressed some of these shortcomings by assessing the proteinaceous composition of kidneys infected with *S. aureus*[14], the current study also examines the temporal and spatial aspects of abscess development.

Various proteomic technologies offer insight into complex biological systems, including the interplay between host and pathogen during infection[15,16]. Recent technological advances have enabled pairing of spatially targeted surface sampling with high-performance mass spectrometry for molecular analysis of tissue. Imaging mass spectrometry (IMS) technology, such as matrix-assisted laser desorption/ionization (MALDI) IMS, offers the unique combination of high molecular specificity and high spatial resolution imaging[17-19]. However, the sensitivity of MALDI IMS for analysis of large proteins (> 30 kDa) can be limited due to low ionization efficiency of proteins from tissue and the poor transmission efficiency of high mass-to-charge ratio (m/z) ions[19,20]. The identification of proteins with MALDI IMS is also challenging due to inefficient fragmentation of low charge state species. To facilitate this process, we have investigated the utility of complementary surface sampling technologies for discovery-based proteomic studies.

Traditional liquid chromatography coupled with tandem mass spectrometry (LC-MS/MS) of peptides derived from proteolytic digestion provides the greatest proteomic sensitivity [21]. LC-MS/MS requires liquid samples, usually through homogenization of tissue, limiting spatial information from the sample of interest. To address this, we recently introduced a spatially targeted, bottom-up proteomics workflow used in analysis of *S. aureus* kidney infection[22]. Specific foci were targeted using picoliter-sized droplets of trypsin protease and the resulting proteolytic peptides were sampled using liquid extraction surface analysis (LESA). The entire process, termed microLESA, is histologically guided using autofluorescence microscopy. Herein, we expand on this work using microLESA to analyze regions from the abscess community (SAC), host-pathogen interface surrounding the community, and regions of cortical tissue of *S.*

aureus infected kidneys. Spatial and temporal proteomic changes were examined by sampling various time points allowing us to follow responses of both the pathogen and the immune system over the course of infection. By studying three defined regions, and their dynamics over the course of the infection, changes in both host and pathogen can be observed across the organ.

Results and Discussion

Identification of bacterial and host proteins in infected tissue

To explore the role of host and bacterial proteins throughout the development of staphylococcal organ abscesses, we analyzed proteins in the abscesses and surrounding areas over time. We focused on kidneys as one of the most commonly utilized model systems for staphylococcal abscess formation. Samples were extracted from one of three defined regions (SAC, interface, and cortex; shown in Fig. 1A) at 4 and 10 dpi (Fig. 1B). These extractions were guided by fluorescence microscopy images (transgenic fluorophore and autofluorescence), which highlights the fluorescent bacterial communities and overall tissue morphology that allowed for differentiation between SAC and adjacent regions. The two time points were selected to ensure sufficient abscess size for extraction, as at 4 dpi abscesses are consistently large enough for micoLESA extraction and at 10 dpi the infection has greatly progressed. We hypothesized that the unique spatial and temporal proteomic analysis would discern i) *S. aureus* physiology and production of virulence determinants within the abscess microenvironment (SAC), ii) onset of the immune response including infection-mediated influx and action of immune cells (interface), as well as iii) organ-wide responses to infection (cortex). A total of 2,399 proteins were identified across all three regions of interest (ROI) and two time points (Table S1 and S2), with an average of 1,153 proteins per time point and ROI (Fig. 1B, Table S1 and S2). Of the proteins detected, 31 were of bacterial origin (Table S2). We identified an additional 26 bacterial proteins that were present in only one set of serial sections or one biological replicate and are not included in Figure 1B due to lower confidence (Table S3). This variability in detection could result from low protein abundance or heterogeneity amongst abscesses, a known challenge when studying

abscess formation[23,24]. Nevertheless, we conclude the identification of these proteins is a strength of the method, as bacterial proteins from *S. aureus* infections are difficult to detect and measure due to ion suppression effects from abundant host proteins within tissues. Since we spatially targeted the abscess region, the inherent 'chemical noise' from the highly abundant host proteins was reduced, greatly improving the sensitivity for the bacterial proteins. Improving the coverage of the bacterial proteome detectable within the tissue microenvironment provided a more complete description of how *S. aureus* molecular machinery contributes to abscess formation and progression.

Bacterial factors

Detection of high abundance proteins related to translation

The microLESA workflow detected 31 bacterial proteins in the defined SAC and interface regions, several of which are involved in the translation process (Fig. 2). These include ribosomal proteins (50S ribosomal proteins L7/L12 [RplL] and L17 [RplQ]), a tRNA-ligase (ThrS) as well as elongation factors Tu (Tuf)[25] and Ts (Tsf)[26]. Several of these intracellular highly abundant proteins were detected in the SAC region and also in the abscess interface (Fig. 2). While we cannot exclude that a small fraction of the bacterial population resides outside of the observable SAC, or the potential for these proteins to 'leak' from the SAC into adjacent regions during the sample preparation process, cell death or autolysin (Atl)-mediated lysis of a staphylococcal subpopulation may cause the release of bacterial factors into the abscess microenvironment[27]. It was previously shown that decreased autolysis by *S. aureus* results in a moderate decrease in renal bacterial numbers in a murine model of systemic infection at 7 dpi[28], supporting the notion that Atl plays a role during for spread to or colonization of this organ. While our data does not allow us to finally conclude why we detect cellular bacterial proteins outside of the SAC, it is intriguing to speculate that (auto)lytic processes are important during abscess formation, potentially aiding infection through the release of intracellular factors.

S. aureus *heme metabolism proteins in the abscess*

153 In response to the presence of *S. aureus* in tissue, the host immune system initiates a variety of anti-bacterial
154 strategies. Nutritional immunity is one such approach in which the immune system limits bacterial access
155 to essential micronutrients (e.g. transition metals) to hinder bacterial growth and stall infection
156 progression[29]. Host-imposed Fe-starvation within the abscess was recently shown by our group using *in*
157 *vivo* imaging and IMS strategies[23,24]. Bacterial pathogens have evolved a number of mechanisms to
158 overcome this Fe limitation[29]. To ensure sufficient levels of the Fe-containing co-factor heme, *S. aureus*
159 imports host heme through the action of the Isd heme uptake system[30]. Additionally, heme can be
160 synthesized *de novo* via a coproporphyrin-dependent bacterial heme biosynthesis pathway[31,32]. In our
161 analysis we observed components of the Isd system (IsdA and IsdB: Fig. 2, Table S2) as well as ChdC
162 (identified with lower confidence, Table S3), a member of the heme biosynthetic pathway, to be present
163 within the abscess[33]. Identification of proteins involved in heme uptake as well as *de novo* heme synthesis
164 suggests that i) *S. aureus* within renal abscesses is indeed heme starved and ii) that multiple strategies are
165 employed to overcome this limitation. These proteins were only detected at 10 dpi (Fig. 2), indicating that
166 metal starvation and corresponding bacterial responses are likely more abundant at later time points during
167 infection.
168
169 *Bacterial factors related to protein stress*
170 Other host-imposed stresses, including production of reactive oxygen species (ROS), reactive nitrogen
171 species (RNS), and elevated temperatures during fever, can damage the bacterial protein pool[34-37]. To
172 protect the staphylococcal proteins from host-derived stresses, bacterial inducible heat shock proteins
173 (Hsps)[38] assist with protein folding and proteostasis[39]. Although this study cannot distinguish between basal
174 and stress-induced expression of such factors, the detection of the major bacterial Hsp DnaK at both the 4
175 dpi and 10 dpi time points (Fig. 2, Table S2) is in accordance with the established roles of Hsps during
176 stress and contact with the host. DnaK is not only involved in maintenance of cellular protein pools, but
177 also plays a role in the folding of *de novo* synthesized proteins, e.g. when adapting to changing
178 environmental conditions[40]. This function is performed in concert with other chaperones, such as the

ribosome-associated intracellular peptidyl prolyl cis/trans isomerase (PPIase)[41], referred to as Trigger factor (TF, Tig)[42], detected in the SAC at 10 dpi (Fig. 2, Table S2). The cooperative nature of these two proteins during stress conditions is demonstrated by both *dnak* and *tig* mutants being viable under laboratory conditions, but a DnaK/TF double mutant being synthetic lethality at temperatures above 30°C. This lethality is likely due to increased protein misfolding under these conditions[42]. In line with the cooperative nature of these proteins, we also found TF to be associated with the SAC at 10 dpi (Fig. 2, Table S2). To our knowledge, the roles of DnaK and TF in *S. aureus* virulence have not been investigated *in vivo*, and it is intriguing to speculate about the importance of these systems during abscess development. The roles of TF are of particular interest, since another *S. aureus* PPIase, PpiB, was previously shown to impact *S. aureus* virulence through a potential function in secretion of nucleolytic and hemolytic proteins[43].

S. aureus *metabolism is shaped by the host environment*

S. aureus can circumvent cellular pathways that have been disrupted by macrophage-derived nitrosative stress[41,44] or hypoxia at sites of infection[45]. Specifically, fermentative pathways[46] can be employed during glucose catabolism under hypoxia or if oxidative phosphorylation is impaired due to the damage of terminal oxidases by radical nitric oxide[47].

Fermentation of pyruvate to lactate by *S. aureus* is facilitated by different lactate dehydrogenases (i.e. Ldh1, Ldh2, Ddh)[46]. We detected Ldh2 in the SAC and interface at 4 and 10 dpi (Fig. 2, Table S2), and Ldh1, a nitric oxide-inducible lactate dehydrogenase, in the abscesses at 4 and 10 dpi, as well as in the interface at 10 dpi (Table S3). It was previously shown that loss of *ldh1* increases staphylococcal sensitivity to nitrosative stress and decreases the ability to form renal abscesses[46]. Furthermore, the additional loss of *ldh2* was found to augment the latter phenotype[46], highlighting the importance of fermentative metabolism for *S. aureus* pathogenicity. In addition to maintaining the cells ability to generate energy under conditions encountered in the abscess, the creation of lactate as a byproduct of fermentation was recently shown to aid in staphylococcal immune evasion[48]. Briefly, bacterial-derived lactate causes alterations of gene expression

in host immune cells, e.g. stimulates the production of the anti-inflammatory cytokine Il-10, allowing for persistence in host tissue. These exciting findings further emphasize how bacterial metabolism shapes to its behavior as a pathogen and ultimately its interaction with the immune system.

Activity of metabolic pathways in *S. aureus* is dependent on environmental conditions and controlled by a large number of transcriptional regulators[49]. Analogously, various regulatory proteins govern pathogenesis of the bacterium[50]. Because the production of the vast array of virulence factors encoded by *S. aureus* is energetically costly, cellular nutritional status and virulence are intimately linked, e.g. through the action of transcriptional regulators that sense and respond to alterations in nutrient availability[51]. A prime example of such a connection is the global transcriptional regulator CodY[52,53]. This bifunctional regulator senses the availability of branched chain amino acids[54,55] and GTP[56], and responds by controlling a large number of metabolic and virulence-related traits. We detected CodY, as only one of two *bona fide* bacterial transcriptional regulators in our dataset, at 4 and 10 dpi in the SAC, and at 10 dpi in the interface (Fig. 2, Table S2). While physical presence of the protein itself is not indicative of its regulatory state, the detection of CodY serves as reminder that *S. aureus* pathophysiology is directly affected by the conditions encountered in the abscess microenvironment, and that sensing of these stimuli guides virulence of the bacterium within the abscess.

S. aureus *secreted proteins*

In addition to the intracellular factors discussed thus far, we identified several staphylococcal proteins that are actively secreted into the abscess environment. Two adhesins belonging to the group of secretable expanded repertoire adhesive molecules (SERAMs)[57] were detected: the extracellular matrix binding protein (Emp)[58,59] and the extracellular adhesion protein (Eap)[60]. Both proteins were among the most consistently observed molecules in the SAC as well as in the interface (Fig. 2, Table S2). Our dataset was manually screened for the presence of Eap as the encoding sequence is found in the USA300 LAC genome, but it is not annotated as a protein. Using this approach, we identified peptides for Eap, indicating

231 production of this protein within host tissue. The presence of Emp and Eap is concurrent with their roles in
232 abscess formation and maintenance[61]. Both proteins were detected in all samples at 4 and 10 dpi, supporting
233 the notion that these factors are abundant and important in both the early and late stages of abscess
234 development[7].
235
236 The action of neutrophils is essential for the immune system to clear staphylococcal infection. Neutrophils
237 are recruited to the site of infection after the recognition of host or pathogen derived factors, including C5a,
238 bacterial formylated peptides, or antimicrobial peptides. Corresponding receptors for these signals are the
239 neutrophil receptor C5aR, the formyl peptide receptor (FPR), and the formyl peptide receptor-like-1
240 (FPRL1)[62,63]. To decrease the negative impact of neutrophil recruitment, *S. aureus* secretes chemotaxis
241 inhibitory proteins that limit the infiltration of immune cells to the site of infection. These secreted factors
242 bind to neutrophil receptors, therefore blocking the recognition of infection-related signal molecules and
243 ultimately preventing neutrophil recruitment. Staphylococcal anti-chemotactic factors include, amongst
244 others[64], the chemotaxis inhibitory protein of *S. aureus* (CHIPS) that antagonizes C5aR and FPR[65], and the
245 FPRL1 inhibitory protein (FLIPr) that blocks the FPRL1 and FPR receptors[66]. Both proteins were identified
246 by our analysis (FLIPr: high confidence, Fig. 2, Table S2; CHIPS: lower confidence, Table S3). Notably,
247 we were only able to detect CHIPS and FLIPr at 10 dpi, suggesting that these factors are expressed or
248 accumulate at advanced stages of abscess development. To our knowledge, this is the first time that
249 production of these chemotaxis inhibitory proteins has been detected by an unbiased *in vivo* screen.
250
251 Another staphylococcal strategy to minimize the impact of the recruited immune cells is the secretion of
252 pore-forming toxins[67]. Upon secretion by *S. aureus*, these proteins insert into and disrupt the plasma
253 membrane of host cells (e.g. neutrophils), ultimately leading to immune cell death. We identified both
254 components of the bi-component leukotoxin LukAB[68,69] (LukA: high confidence, LukB: lower confidence)
255 at 10 dpi (Fig. 2, Tables S2 and S3). Presence of these proteins was recently correlated to abscess formation,
256 further validating our method[68]. LukB, as well as several other proteins identified by our microLESA

approach (i.e. Chp, Emp and Eap) are expressed under the control of the major virulence regulatory system SaeRS[70], whose activity can be modulated in response to host-derived signals (e.g. Zn-bound calprotectin or human neutrophil peptides)[71,72]. These results indicate that the SaeRS system may be active during adaptation to the abscess microenvironment and further highlight the interconnected nature of the host-pathogen interface, where the actions of host and bacteria are inseparably intertwined.

Host-derived factors

Spatial and Temporal Changes in the Host Proteome

The majority of proteins identified in this study were of host origin. The large number of murine proteins detected (2,368) allowed for the probing of the relationships between different tissue regions as well as the determination of the proteomic changes within regions over time. At 4 dpi, the majority of identified proteins (676) are common among all three regions. This suggests that 4 days may not be sufficient for the full immune response to be observed and proteinaceously distinct abscess regions to form. The most unique region at this time point is the SAC (Fig. 3). The SAC region also displayed the least changes over the course of infection, where the vast majority of proteins in the region were present at both time points (964, Figure 3B). This indicates that once an abscess community has been formed, the makeup of this region appears to remain fairly stable. At 4 dpi the interface and SAC show high degrees of similarity with an overlap of 211 proteins. As the infection progresses this overlapping region becomes one of the most prominent groups represented in our dataset (635) after proteins unique to the cortex (657), while the overlap between all three regions is less than at 4 dpi (441 vs. 676). This indicates that as the infection continues, the site of infection (SAC and interface) and the cortex grow increasingly more distinct. As depicted in Figure 3B, only half of the proteins detected in the cortex were found at 4 and 10 dpi, which is in stark contrast to the trend seen in the SAC. These large-scale changes in the cortex suggest organ-wide effects of infection by *S. aureus*. We hypothesize that this increase in unique proteins in the cortex is likely

due to the resolution of the immune response, in regions that are not in direct contact with the pathogen. This hypothesis is discussed further in the host response section regarding metabolism.

Amongst the different investigated regions, the most notable trends are in the interface. The number of unique proteins detected only in the interface showed dramatic change over the course of the experiment, increasing greater than ten-fold from 4 dpi (36 proteins) to 10 dpi (384 proteins) as shown in Fig. 3. Additionally, many of the proteins found in the SAC at 4 dpi are shared with the interface by 10 dpi (635 proteins), suggesting that the interface becomes a major site of the competition between host and pathogen. The finding that many proteins were uniquely detected at the interface suggests that we are able to assess the proteome of this region without unwanted contamination from neighboring regions. In the case of unintended cross-contamination between the SAC and the interface, host proteins would likely be common between the two regions leading to a similar makeup, which was not observed in this data set. These findings also support the observation of bacterial cytosolic proteins detected at the interface indeed is biologically relevant and not merely an artifact of sample acquisition. Our results indicate that the interface is a unique and deeply informative tissue environment for understanding staphylococcal pathogenesis.

Immune cell distributions

Similar to the rich biology seen from our analysis of bacterial proteins, thousands of identified murine proteins characterize the host response to *S. aureus* infection. A summary of all identified host-derived proteins, including information about localization and time of identification, can be found in Table S1. Consistent with a predicted presence of immune cells in the abscess, the pan-leukocyte marker Receptor-type tyrosine-protein phosphatase C (Ptprc or CD45) is present in the SAC and interface at 4 and 10 dpi (Fig. 4). Curiously, other proteins thought to be specifically expressed by cells of hematopoietic lineages do not follow the same pattern as CD45. Lymphocyte-specific protein 1 (Lsp1) is also found in the cortical regions of the kidney both 4 and 10 dpi, while dedicator of cytokinesis protein 2 (Dock2) is only found in

the abscess and interface 10 dpi (Fig. 4). This suggests subtle spatial and temporal differences in the leukocyte populations during infection.

During abscess formation, neutrophils are recruited to the site of infection in high numbers[73-75]. We identified the myeloid cell marker CD14 and neutrophil marker CD177 within the abscess and interface (Fig. 4). Coinciding with the neutrophil surface markers, multiple neutrophil-specific antimicrobial factors are also found in the abscess and interface regions including myeloperoxidase (Mpo), cathepsin G (Ctsg), and neutrophil elastase (Elane) (Fig. 4). In addition, neutrophils use NADPH oxidase to generate high levels of ROS in response to *S. aureus*, and an abundance of NADPH oxidase proteins are also specifically within the abscess and interface. The inducible nitric oxide synthase (Nos2), however, is only found in the abscess 4 dpi (Fig. 4). While it is not possible to fully exclude that Nos2 is present in low concentrations below our limit of detection at this later time point, Nos2 was reliably detected in nearly all samples at the 4 dpi time point. This suggests that even if Nos2 is not absent from the abscess at 10 dpi, the concentration decreases over time.

Relative to neutrophils, macrophages make up a smaller percentage of the immune cells in the abscess[76]. Nevertheless, the presence of integrin alpha-M (Itgam or Mac-1) indicates that activated inflammatory macrophages are found in the abscess and interface (Fig. 4). The expression of apolipoprotein B receptor (Apobr) by macrophages is critical to combating *S. aureus*, as it suppresses activation of the Agr system, a major component of the staphylococcal regulatory landscape[76] (Fig. 4). Consistent with an integral role in combating *S. aureus*, Apobr is present both within the abscess and interface at 4 and 10 dpi. The presence of sortilin-related receptor (Sorl1), and mannose-6-phosphate receptor (M6pr) at 10 dpi in the cortex suggests the presence of alternatively activated M2-like macrophages involved in tissue repair and remodeling outside of the abscess (Fig. 4). The classical M2-like macrophage marker arginase-1 (Arg1) is not detected in the cortex and is present ubiquitously in the abscess and interface (Fig. 4). Despite Arg1

being linked to M2 polarization, Arg1 is only produced by a quarter of all M2-like macrophages[77] and is furthermore up-regulated in inflammatory M1-like macrophages[78,79]. Arg1 is necessary for the production of spermine and spermidine, which are uniquely toxic to most methicillin-resistant *S. aureus* (MRSA) strains and integral to killing *S. aureus* during the tissue resolution phase of skin infections[80]. The presence of spermidine synthase (Srm) in the abscess at 4 dpi suggests spermine and spermidine production may play a critical antimicrobial function within abscesses in the kidney[81] (Fig. 4). These data suggest that during *S. aureus* infection of kidneys, Arg1 may be present in M1 macrophages in the abscess and might not be a reliable marker for the M2 macrophages associated with tissue repair in the cortex 10 dpi.

Heme distribution

Heme acts as a critical source of iron for *S. aureus* at the site of infection[82]. While hemoglobin subunit alpha (Hba) and beta-1 (Hbb-b1) are ubiquitously present during infection, hemoglobin subunit beta-2 (Hbb-b2) and beta-H0 (Hbb-b0) are only found in the cortex at 10 dpi (Fig. 4). Importantly, the host can restrict free heme and hemoglobin from *S. aureus* through binding and sequestration by hemopexin (Hpx)[83] and haptoglobin (Hp)[84], respectively. Both Hpx and Hp were found in the abscess, interface, and cortex at 4 dpi, but not in the cortex at 10 dpi (Fig. 4). This suggests that while free heme and hemoglobin may be present at the site of infection in the kidney, the simultaneous presence of Hpx and Hp may render heme and hemoglobin biologically unavailable to *S. aureus*. The presence of host factors that limit heme availability to *S. aureus* also serve as an explanation for the previously discussed presence of different staphylococcal proteins aimed to counteract heme limitation during infection (i.e. IsdA, IsdB and ChdC) (Fig. 2). Another heme-containing protein, cytoglobin (Cygb), is exclusively present in the cortex at 10 dpi. Cygb contributes to oxygen diffusion for collagen synthesis during wound healing[85], regulating nitric oxide levels[86,87] and detoxifying reactive oxygen species[88] (Fig. 4). Cygb mirrors the presence of M2 macrophages in the cortex at 10 dpi, that suggests Cygb plays a role in tissue repair and abscess resolution during *S. aureus* infection.

Host signaling

The power of microLESA is not just in confirming the presence or absence of proteins, but in allowing for unbiased observations about the regulatory states of the cells. NEDDylation and ubiquitylation are posttranslational modifications that regulate protein degradation by the proteasome, thereby influencing signal transduction[89-94], inflammasome activation[95,96,97], autophagy[98,99], and cell death[100,101]. The cullin-associated NEDD8-dissociated protein 1 (Cand1) regulates NEDD8 activity by sterically inhibiting the assembly of cullin-RING ubiquitin ligases and preventing NEDDylation[102], while the NEDD8 ultimate buster 1 (Nub1) specifically recruits NEDD8 to the proteasome for degradation[103,104]. In the abscess, interface (both at 4 and 10 dpi), and cortex (at 4 dpi) Cand1 was present and Nub1 absent, suggesting that NEDDylation is being regulated by Cand1 (Fig. 4). However, in the cortex at 10 dpi, the phenotype reversed with the presence of Nub1, and absence of Cand1, suggesting that NEDDylation is impaired by the Nub1-mediated degradation of NEDD8. The reduction of total NEDD8 protein would have significant implications in multiple signal transduction pathways, including NFκB and HIF1α, and suggests the signaling environment within the cortex at 10 dpi is unique. Enzymes necessary for ubiquitination and proteasomal degradation of proteins, including the ubiquitin activating enzymes (E1) that catalyze the first step in the ubiquitination reaction, and ubiquitin ligases (E3) that catalyze the transfer of ubiquitin from the E2 enzyme to the protein substrate, show similar spatial and temporal patterns. Since, E1 and E3 enzymes interact directly with the protein substrate, it is possible that varying complexes of E1, E2, and E3 enzymes exhibit unique activities to exert diverse biological functions (Table S1).

Host metabolism: Glycolysis and glucogenesis

Not only does signal transduction vary spatially and temporally, but the metabolic niche changes at different renal locations when comparing 4 and 10 dpi (Fig. 4 and S2). We utilized a systems biology pathway analysis tool, SIMONE, to visualize the interactions between proteins of interest (Fig. S3). These proteins were determined using external pathway mapping tools, entered into Reactome[105] and the resulting list of

384 proteins associated with metabolism were input into SIMONE[106] as seed proteins. This tool constructs
385 networks using the MAGINE framework[107], which derives protein connection information from multiple
386 databases (Fig. S2). By uncovering how these proteins are connected, pathways can be predicted from
387 spatiotemporal proteomics data. These pathways were summarized and combined in Figure 5. While we
388 observed alterations in abundance of various proteins related to different metabolic processes (discussed
389 below), the enzymes necessary for glycolysis are generally present during infection in the abscess, interface,
390 and cortex, suggesting glucose conversion to pyruvate. Many of the enzymes necessary for the pentose
391 phosphate pathway that runs parallel to glycolysis and enzymes necessary to breakdown fructose that feed
392 into glycolysis are not detected in the cortex at 10 dpi. However, the enzyme bisphosphoglycerate mutase
393 (Bpgm) is solely present in the cortex. This enzyme is necessary to form 2,3-bisphosphoglycerate from the
394 glycolysis intermediate 1,3-bisphophoglycerate. The absence of Bpgm in the abscess and interface is
395 consistent with a hypoxic environment in the abscess, as 2,3-bisphosphoglycerate binds hemoglobin at a
396 high affinity and causes a conformational change resulting in the release of oxygen[108,109] (Fig. 5 and S2).
397
398 The enzymes necessary for host gluconeogenesis, a process that converts non-carbohydrate substrates into
399 glucose, were only detected in the abscess and cortex at 4 dpi, suggesting that gluconeogenesis may not
400 occur late in infection (Fig. 5 and S2). The enzymes necessary for glycogenolysis are present in the abscess,
401 interface, and cortex; however, glycogen synthase kinase-3 alpha (Gsk3a), an enzyme that contributes to
402 glycogenesis, is not detected in the abscess and interface (Fig. 5 and S2). The lack of enzymes for glucose
403 formation and long-term storage in the form of glycogen, and the presence of enzymes necessary for the
404 breakdown of glycogen into glucose in the abscess and interface is consistent with high levels of glycolysis
405 during inflammation (reviewed in[110]). The presence of Gsk3a exclusively in the cortex at 10 dpi suggests a
406 decreased metabolic demand for glucose and possible glycogen formation. In addition, Gsk3a plays a
407 central role in regulating the transition between pro-inflammatory and immune-suppressive response to *S.*
408 *aureus* by controlling cytokine production[111]. These results suggest a specific role for Gsk3a in altering the
409 metabolic and cytokine landscape of the cortex 10 dpi during *S. aureus* infection of the kidney.

Host Metabolism: Metabolism in the abscess

While the metabolic enzymes present in the abscess and interface suggest the formation of pyruvate, the complex necessary for conversion of pyruvate into acetyl coenzyme A (acetyl-CoA) in the mitochondria may not be fully formed. Pyruvate dehydrogenase protein X component (Pdhx) tethers the E3 dimers to the E2 core of the pyruvate dehydrogenate complex[112,113] (Fig. 5 and S2). Therefore, lacking detectable Pdhx in the abscess and interface suggests that the pyruvate dehydrogenase complex would not be functional and that conversion of pyruvate into acetyl-CoA in the mitochondria would be impaired. Pyruvate can also be converted into acetyl-CoA in the cytosol[114], but the acetyl-coenzyme A synthetase (Acss2), which is necessary for transport into the mitochondria, is also not detected within the abscess and interface (Fig. 5 and S2). Instead, the ubiquitous expression of the lactate dehydrogenase (Ldha and Ldhb) suggests that in the abscess and interface, the resulting pyruvate from glycolysis is being converted to lactate, consistent with anaerobic glycolysis in the hypoxic environment of the abscess (Fig. 5 and S2).

Many of the enzymes associated with the tricarboxylic acid (TCA) cycle are present in the abscess and interface during infection, but pyruvate does not seem to be fueling downstream oxidative phosphorylation and ATP generation due to the lack of Pdhx and Acss2 (Fig. 5 and S2). Many of the enzymes necessary for β-oxidation in the mitochondria are present in the abscess and interface, and the resulting formation of acetyl-CoA could fuel the TCA cycle (reviewed[115]). However, long-chain fatty acids (LCFAs) would likely not be able to serve as the carbon source for the TCA cycle. The O-palmitoyltransferase 2 (Cpt2), catalyzes the formation of palmitoyl-CoA from palmitoylcarnitine, a necessary step for LCFAs prior to β-oxidation (reviewed in[115]). Thus, the lack Cpt2 suggest that LCFAs cannot undergo β-oxidation in the mitochondria and therefore are not feeding into the TCA cycle in the abscess and interface (Fig. 5 and S2). This does not exclude the possibility that short-chain fatty acids (SCFAs), which passively gain access to the mitochondria, could be fueling the TCA cycle. Carnitine O-acetyltransferase (Crat) blunts acetyl-CoA from fueling the TCA cycle by forming acetyl-carnitine for transport into the cytosol, and once in the cytosol,

436 acylcarnitine hydrolase (Ces2c) liberates fatty acids from L-carnitine. Both Crat and Ces2c are absent in
437 the in the abscess and interface supporting the possibility that SCFAs undergoing β-oxidation could serve
438 as a carbon source for the TCA cycle (Fig. 5 and S2). Glutamine may also act as an alternative carbon
439 source for the TCA cycle [116]. Glutamate dehydrogenase 1 (Glud1) catalyzes the oxidative deamination of
440 glutamate into α-ketoglutarate, which feeds into the TCA cycle. The presence of Glud1 and absence of
441 glutamine synthase (Glul), which converts glutamate into glutamine, in the abscess and interface suggests
442 that glutamine may also be fueling the TCA cycle in the abscess environment (Fig. 5 and S2).
443
444 *Host Metabolism: Metabolism in the cortex*
445 By contrast, in the cortex at 10 dpi many of the enzymes necessary to run the TCA cycle are not detected.
446 Only isocitrate dehydrogenase (Idh2), NAD-dependent malic enzyme (Me2), and malate dehydrogenase
447 (Mdh2) are detected (Fig. 5 and S2), suggesting that in the cortex at 10 dpi, the full TCA cycle may not be
448 used. The cortex at 10 dpi is the only region to contain all the acyl-CoA dehydrogenases as well as almost
449 exclusive presence of the enzymes necessary for β-oxidation in the peroxisome. Unlike the abscess and
450 interface, Cpt2, is detected in the cortex suggesting that β-oxidation of LCFAs may occur, but the presence
451 of Ces2c and Crat suggest that the resulting acetyl-CoA is shunted out of the mitochondria rather than
452 feeding into the TCA cycle. M2 macrophages in the tissue surrounding the abscess (Fig. 5 and S2) are
453 necessary for the conversion to the resolution phase by cleaning up apoptotic cells and cellular debris, and
454 are consistent with previous studies assessing abscess biology in the skin and soft tissue[80]. Cellular debris
455 contains high concentrations of lipids, thereby requiring β-oxidation for its degradation. The high presence
456 of lipids in resolving damaged tissue outside the abscess could account for the increased presence of
457 proteins necessary for β-oxidation.
458
459 Acetyl-coenzyme A synthetase 2-like (Acss1) and malonyl-CoA decarboxylase (Mlycd) are also present in
460 the cortex 10 days-post infection (Fig. 5 and S2). These enzymes shunt mitochondrial acetate and malonyl-
461 CoA away from lipid synthesis and toward the formation of acetyl-CoA. The combined activity of β-

462 oxidation, Acss1, and Mlycd with a limited presence of TCA cycle enzymes could cause an accumulation
463 of acetyl-CoA. The presence of Crat and Cesc2c may relieve some of the acetyl-CoA burden by exporting
464 acetyl-CoA as free fatty acids into the cytosol. Alternatively, many of the enzymes necessary for
465 ketogenesis are present in the cortex at 10 dpi suggesting that the abundance of acetyl-CoA could also be
466 converted to ketone bodies (Fig. 5 and S2).
467
468 A byproduct of β-oxidation is oxidative stress, and consistent with increased β-oxidation, the cortex at 10
469 dpi is the only region to express the full array of glutathione S-transferases, synthase, reductase, and
470 peroxidase to combat oxidative stress (Table S1). Since oxidative phosphorylation from the TCA cycle can
471 create oxidative stress, this could explain the absence of TCA cycle enzymes in the cortex at 10 dpi (Fig. 5
472 and S2). Finally, many of the downstream enzymes for β-oxidation in the mitochondria and peroxisome are
473 not detected in the cortex at 10 dpi that are present at 4 days or in the abscess and interface (Fig. 5 and S2).
474 This suggests that while β-oxidation of LCFAs is occurring in the cortex at 10 dpi, the lipids are not fully
475 broken down. In addition, acyl-coenzyme A thioesterases (Acot) are thought to maintain a sufficient CoA
476 pool for β-oxidation by terminating β-oxidation after a set number of cycles (reviewed in[117]). The specific
477 presence of Acot4 in the peroxisome and Acot9 and Acot13 in the mitochondria could result in the
478 formation of specific lipid products that is important in maintaining β-oxidation in high lipid environments
479 in order to avoid oxidative stress (Fig. 5 and S2). The metabolic environment in the cortex at 10 dpi is
480 consistent with an immune response that has altered to a resolving phase that is cleaning up lipid-dense
481 apoptotic cells and cellular debris following inflammation.
482
483 **Summary**
484 We performed spatially and temporally targeted proteomics, aided by a robust systems biology data
485 processing workflow, to molecularly investigate staphylococcal abscess formation and development. This
486 approach is suited to reliably identify bacterial proteins as well as enables characterization of the host
487 proteome during infection. Such a comprehensive assessment of the entire abscess proteome allows us to

488 molecularly characterize the host-pathogen interface over time. By pairing information about the
489 spatiotemporal distribution of bacterial proteins with data defining the host proteome, we can elucidate how
490 pathogen and host shape the abscess (micro)environment and how, in turn, both parties react to these
491 biomolecular changes.
492
493 Using our microLESA workflow, we characterized the metabolic niche at the site of infection. Our findings
494 indicate the influx of immune cells (i.e. neutrophils and different macrophage populations), while also
495 elucidating specific metabolic processes employed by these host cell populations. The action of
496 macrophages was not limited to the SAC and interface. We also detected markers for M2 macrophages in
497 the renal cortex, suggesting a role in tissue repair and remodeling. In contrast, multiple neutrophil-specific
498 antimicrobial factors (e.g. Mpo, Ctsg, Elane) were found to be expressed in proximity to the staphylococcal
499 abscess. We found *S. aureus* produces CHIPS and FLIPr, which antagonize the host neutrophil receptors
500 to prevent neutrophilic entrance into the abscess. Staphylococcal leukotoxins (LukAB) produced during
501 abscess formation were also identified, again aiding in immune evasion and persistence in the host tissue.
502 Indicative for the onset of nutritional immunity, we observed bacterial heme uptake and biosynthetic
503 proteins present in the abscess. This limitation could be explained by the presence of host proteins that
504 restrict the availability of heme for *S. aureus* (Hpx and Hp), particularly in the SAC and interface.
505
506 We describe several other additional mechanisms of how host and pathogen directly affect each other during
507 infection and how both sides counteract the challenges presented to them. These data highlight the powerful
508 nature of our experimental setup and offer insights into the processes at the host-pathogen interface, beyond
509 the specific examples discussed here. The ability to elucidate when, where and how pathogens and immune
510 systems interact during abscess formation and disease progression, is an invaluable resource to identify
511 potential points of intervention when developing new anti-staphylococcal therapeutic strategies.
512

Materials and Methods

Murine model of systemic S. aureus infection

6-8 week old female C67BL/6J mice were anesthetized with tribromoethanol (Avertin) and retro-orbitally infected with ~1.5-2 x 10^7 CFUs of *S. aureus* USA300 LAC constitutively expressing sfGFP from the genome (P*sarA*-sfGFP integrated at the SaPI1 site)[22]. Infections were allowed to progress for 4 or 10 days before animals were humanely euthanized and organs removed for subsequent analysis.

Chemicals

Acetonitrile, acetic acid, formic acid, trifluoracetic acid, ethanol, ammonium bicarbonate, and chloroform were purchased from Fisher Scientific (Pittsburgh, PA). Mass spectrometry sequence-grade trypsin from porcine pancreas was purchased from Sigma-Aldrich Chemical, Co. (St. Louis, MO).

Micro-Digestions

All sample preparation was completed using the method previously described by Ryan *et al.*[22]. Excised murine kidneys infected with *S. aureus* USA300 LAC carrying a constitutive fluorescent reporter were fresh frozen on dry ice and stored at -80°C. Tissues were then cryosectioned at 10 µm thickness (Leica Microsystems, Buffalo Grove, IL) and thaw mounted onto custom fiducial microscope slides (Delta Technology, Loveland, CO). For all samples, an autofluorescence microscopy image (Carl Zeiss Microscopy, White Plains, NY) was acquired at 10x magnification (0.92 µm/pixel) prior to spotting using FITC and DAPI filters (FITC excitation λ, 465-495 nm; emission λ, 515-555 nm; DAPI excitation λ, 340-380 nm; emission λ, 435-485 nm). Microscopy exposure time was set to 200 ms for the DAPI filter and 100 ms for the FITC filter. Samples were washed with graded ethanol washes for 30s (70% EtOH, 100% EtOH, Carnoy's Fluid, 100% EtOH, H2O, 100% EtOH) and Carnoy's fluid for 3min (6 ethanol: 3 chloroform: 1 acetic acid) to remove salts and lipids. Samples were allowed to dry under vacuum prior to trypsin digestion. Regions targeted for digestion were annotated on microscopy images using ImageJ (U.S.

National Institutes of Health, Bethesda, MD) and converted into instrument coordinates for the piezoelectric spotter using an in-house script (Fig. S1). Trypsin was dissolved in ddH_2O to a final concentration of 0.048 µg/mL. A piezoelectric spotting system (sciFLEXARRAYER S3, Princeton, NJ) was used to dispense ~250 pL droplets of trypsin. Trypsin was dispensed on regions of interest (ROIs) 20 times with one drop per run in order to reduce spot size, with 4 spots per ROI. The four trypsin spots were positioned so that all tryptic peptides for an ROI could be collected using a single LESA experiment. Following trypsin deposition, samples were incubated at 37°C for three hours in 300 µL ammonium bicarbonate.

LESA

Liquid surface extraction was completed using a TriVersa NanoMate (Advion Inc., Ithaca, NY) with the LESAplusLC modification. Digested samples were scanned using a flatbed scanner and uploaded to the Advion ChipSoft software. 5 µL of extraction solvent (2:8 acetonitrile/water with 0.1% formic acid) was aspirated into the glass capillary. The capillary was then lowered to a height of approximately 0.5 mm above the sample surface and 2.5 µL of solvent was dispensed onto ROIs. Contact with the surface was maintained for 10s and 3.0 µL of solvent was re-aspirated into the capillary. The initial 5 µL volume was dispensed into a 96-well plate containing 200 µL of water/0.1% formic acid. The LESA extraction was repeated twice at the same ROI and combined. Three wash cycles of the instrument were completed between each ROI set to prevent carryover from other biological regions. Resulting extracts were then dried down under vacuum and stored at -80˚C until LC-MS/MS analysis.

LC-MS/MS

Dried peptide samples were reconstituted in 10 µL of water/0.1% formic acid prior to analysis. Tryptic peptides from tissue extracts were injected and gradient eluted on a pulled tip emitter column packed in-house with C18 material (Waters BEH C18). The column was heated to 60˚C with a flow rate of 400 nL/min using an Easy-nLC 1000 UHPLC (Thermo Scientific, San Jose, CA). Mobile phase A consisted of H_2O with 0.1% formic acid, and mobile phase B consisted of acetonitrile with 0.1% formic acid. Peptides were

565 eluted on a linear gradient of 2-20% B for 100 minutes, followed by 20-32% B for 20 minutes, and lastly
566 32-95% B for one minute. Eluting peptides were analyzed using an Orbitrap Fusion Tribrid mass
567 spectrometer (Thermo Scientific, San Jose, CA). MS1 scans were acquired at 120,000 resolving power at
568 *m/z* 200 using the Orbitrap, with a mass range of *m/z* 400-1600, and an automatic gain control target of
569 $1.0x10^6$.
570
571 *Data Analysis*
572 For peptide identification, tandem mass spectra were searched using Protalizer software (Vulcan Analytic,
573 Birmingham, Alabama) and MaxQuant[118] against a database containing both the mouse and *S. aureus* strain
574 USA300 LAC proteome created from the UniprotKB[119]. Modifications such as glycosylation,
575 phosphorylation, methionine, oxidation, and deamidation were included in the Protalizer database search
576 with an FDR of 1%. For MaxQuant analysis, raw files were processed using a label-free quantification
577 method implemented in MaxQuant version 1.6.7. Spectra were searched against mouse and *Staphylococcus*
578 *aureus* (strain USA300) reference databases downloaded from UniProt KB. These were supplemented with
579 the reversed sequences and common contaminants automatically (decoy database) and used for quality
580 control and estimation of FDR by MaxQuant. Carbamidomethylation was set as a fixed modification and
581 acetyl (protein N-term) and oxidation (M) were set as variable modifications. Minimal peptide length was
582 7 amino acids. Peptide and protein FDRs were both set to 1%. The resultant protein groups file from
583 MaxQuant was analyzed for outliers by calculating z-scores for each sample based on number of protein
584 groups identified; 3 samples out of 42 were excluded as outliers. Proteins identified as “reverse”, “only
585 identified by site”, or “potential contaminants” were also removed.
586 Proteins identified by Protalizer and MaxQuant were filtered based on the following criteria: 2
587 unique peptides contributed to the protein identification, proteins were detected in 2+ biological replicates,
588 and proteins were detected in 2+ serial sections. Bacterial proteins also met these criteria, with the exception
589 of those listed in Table S3 (designated as ‘lower confidence’) that only met 1 of the 2 replicate requirements
590 criteria but did meet the 2+ unique peptide criteria. We believe these proteins did not fulfil the requirements

for high confidence due to potentially relevant differences in abundance or due to heterogeneity between abscesses. Since these proteins have previously been studied in a primarily targeted manner rather than our discovery-based approach, we include these data but additional confirmation is required. The lists generated by each dataset were cross compared for all proteins, to aid in identification from the protein groups generated by MaxQuant. Tables S1 and S2 include the full list of identified proteins, and include the search algorithm(s) were used for identification

Pathway analysis was conducted using a similar workflow described previously by Gutierrez and colleagues[106]. Briefly, data were uploaded into a central in-house database and organized by identifiers such as tissue location and infection time. Project data were exported into a custom data analysis and visualization tool for network construction (SIMONE) in a data driven manner. Data was entered into Reactome[105], a free online pathway mapping software, and proteins associated with metabolism were selected from the Reactome output. The genes encoding for these proteins were then input into the network construction software as root nodes. Network construction was performed as described[107] in conjunction with a custom user interface that provided visualization (through the use of Cytoscape24) of the constructed data networks. Resulting networks are shown in Fig. S1 and S2.

Data and Software Availability

The mass spectrometry proteomics data have been deposited to the ProteomeXchange Consortium via the PRIDE[120] partner repository with the dataset identifier PXD019920.

Acknowledgements

This work was funded by the NIH National Institute of Allergy and Infectious Diseases (R01AI138581 awarded to E.P.S and J.M.S. and R01AI069233, R01AI073843 awarded to E.P.S.) and NIH National Institute of General Medical Sciences (2P41 GM103391-07 awarded to R.M.C.). A.W. is supported by American Heart Association (18POST33990262) and the NIH National Institute of Environmental Health Sciences (T32ES007028).

Author Contributions

E.R.G., A.W., A.J.M, D.B.G., R.M.C., E.P.S., J.M.S wrote the manuscript. A.W. performed animal infection models. W.J.P aided with sample preparation. D.J.R. designed experiments and collected data. E.R.G. and K.S. performed data analysis and pathway-mapping results.

Conflict of Interest

The authors declared that they have no conflict of interest.

Literature

1 Laupland, K. B. Defining the epidemiology of bloodstream infections: the 'gold standard' of population-based assessment. *Epidemiol Infect* **141**, 2149-2157, doi:10.1017/S0950268812002725 (2013).

2 Klein, E. Y. *et al.* National Costs Associated With Methicillin-Susceptible and Methicillin-Resistant *Staphylococcus aureus* Hospitalizations in the United States, 2010-2014. *Clin Infect Dis* **68**, 22-28, doi:10.1093/cid/ciy399 (2019).

3 van Hal, S. J. *et al.* Predictors of mortality in *Staphylococcus aureus* Bacteremia. *Clin Microbiol Rev* **25**, 362-386, doi:10.1128/CMR.05022-11 (2012).

4 Fowler, V. G., Jr. *et al.* Clinical identifiers of complicated *Staphylococcus aureus* bacteremia. *Arch Intern Med* **163**, 2066-2072, doi:10.1001/archinte.163.17.2066 (2003).

5 Cheng, A. G., DeDent, A. C., Schneewind, O. & Missiakas, D. A play in four acts: *Staphylococcus aureus* abscess formation. *Trends Microbiol* **19**, 225-232, doi:10.1016/j.tim.2011.01.007 (2011).

6 Guggenberger, C., Wolz, C., Morrissey, J. A. & Heesemann, J. Two distinct coagulase-dependent barriers protect *Staphylococcus aureus* from neutrophils in a three dimensional in vitro infection model. *PLoS Pathog* **8**, e1002434, doi:10.1371/journal.ppat.1002434 (2012).

7 Cheng, A. G. *et al.* Genetic requirements for *Staphylococcus aureus* abscess formation and persistence in host tissues. *FASEB J* **23**, 3393-3404, doi:10.1096/fj.09-135467 (2009).

8 Lam, G. T., Sweeney, F. J., Jr., Witmer, C. M. & Wise, R. I. Abscess-Forming Factor(S) Produced by *Staphylococcus Aureus*. Ii. Abscess Formation and Immunity by a Staphylococcus and Its Mutants. *J Bacteriol* **86**, 87-91 (1963).

9 Cheng, A. G. *et al.* Contribution of coagulases towards *Staphylococcus aureus* disease and protective immunity. *PLoS Pathog* **6**, e1001036, doi:10.1371/journal.ppat.1001036 (2010).

10 Chen, P. R. *et al.* An oxidation-sensing mechanism is used by the global regulator MgrA in *Staphylococcus aureus*. *Nat Chem Biol* **2**, 591-595, doi:10.1038/nchembio820 (2006).

11 Rauch, S. *et al.* Abscess formation and alpha-hemolysin induced toxicity in a mouse model of *Staphylococcus aureus* peritoneal infection. *Infect Immun* **80**, 3721-3732, doi:10.1128/IAI.00442-12 (2012).

12 Kobayashi, S. D., Malachowa, N. & DeLeo, F. R. Pathogenesis of *Staphylococcus aureus* abscesses. *Am J Pathol* **185**, 1518-1527, doi:10.1016/j.ajpath.2014.11.030 (2015).

13 Corbin, B. D. *et al.* Metal chelation and inhibition of bacterial growth in tissue abscesses. *Science* **319**, 962-965, doi:10.1126/science.1152449 (2008).

14 Attia, A. S. *et al.* Analysis of the *Staphylococcus aureus* abscess proteome identifies antimicrobial host proteins and bacterial stress responses at the host-pathogen interface. *Pathog Dis* **69**, 36-48, doi:10.1111/2049-632X.12063 (2013).

15 Zhang, C. G., Chromy, B. A. & McCutchen-Maloney, S. L. Host-pathogen interactions: a proteomic view. *Expert Rev Proteomics* **2**, 187-202, doi:10.1586/14789450.2.2.187 (2005).

16 Schmidt, F. & Volker, U. Proteome analysis of host-pathogen interactions: Investigation of pathogen responses to the host cell environment. *Proteomics* **11**, 3203-3211, doi:10.1002/pmic.201100158 (2011).

17 Buchberger, A. R., DeLaney, K., Johnson, J. & Li, L. Mass Spectrometry Imaging: A Review of Emerging Advancements and Future Insights. *Anal Chem* **90**, 240-265, doi:10.1021/acs.analchem.7b04733 (2018).

18 Shariatgorji, M., Svenningsson, P. & Andren, P. E. Mass spectrometry imaging, an emerging technology in neuropsychopharmacology. *Neuropsychopharmacology* **39**, 34-49, doi:10.1038/npp.2013.215 (2014).

19 Spraggins, J. M. *et al.* Next-generation technologies for spatial proteomics: Integrating ultra-high speed MALDI-TOF and high mass resolution MALDI FTICR imaging mass spectrometry for protein analysis. *Proteomics* **16**, 1678-1689, doi:10.1002/pmic.201600003 (2016).

20 Liu, Z. & Schey, K. L. Fragmentation of multiply-charged intact protein ions using MALDI TOF-TOF mass spectrometry. *J Am Soc Mass Spectrom* **19**, 231-238, doi:10.1016/j.jasms.2007.06.006 (2008).

21 Zhang, Y., Fonslow, B. R., Shan, B., Baek, M. C. & Yates, J. R., 3rd. Protein analysis by shotgun/bottom-up proteomics. *Chem Rev* **113**, 2343-2394, doi:10.1021/cr3003533 (2013).

22 Ryan, D. J. *et al.* MicroLESA: Integrating Autofluorescence Microscopy, *In Situ* Micro-Digestions, and Liquid Extraction Surface Analysis for High Spatial Resolution Targeted Proteomic Studies. *Anal Chem* **91**, 7578-7585, doi:10.1021/acs.analchem.8b05889 (2019).

23 Cassat, J. E. *et al.* Integrated molecular imaging reveals tissue heterogeneity driving host-pathogen interactions. *Sci Transl Med* **10**, doi:10.1126/scitranslmed.aan6361 (2018).

24 Perry, W. J. *et al. Staphylococcus aureus* exhibits heterogeneous siderophore production within the vertebrate host. *Proc Natl Acad Sci U S A* **116**, 21980-21982, doi:10.1073/pnas.1913991116 (2019).

25 Widjaja, M. *et al.* Elongation factor Tu is a multifunctional and processed moonlighting protein. *Sci Rep* **7**, 11227, doi:10.1038/s41598-017-10644-z (2017).

26 Miller, D. L. & Weissbach, H. Interactions between the elongation factors: the displacement of GPD from the TU-GDP complex by factor Ts. *Biochem Biophys Res Commun* **38**, 1016-1022, doi:10.1016/0006-291x(70)90341-4 (1970).

27 Pasztor, L. *et al.* Staphylococcal Major Autolysin (Atl) Is Involved in Excretion of Cytoplasmic Proteins. *Journal of Biological Chemistry* **285**, 36794-36803, doi:10.1074/jbc.M110.167312 (2010).

28 McCarthy, H. *et al.* The major autolysin is redundant for *Staphylococcus aureus* USA300 LAC JE2 virulence in a murine device-related infection model. *FEMS Microbiol Lett* **363**, doi:10.1093/femsle/fnw087 (2016).

29 Hood, M. I. & Skaar, E. P. Nutritional immunity: transition metals at the pathogen-host interface. *Nat Rev Microbiol* **10**, 525-537, doi:10.1038/nrmicro2836 (2012).

30 Skaar, E. P. & Schneewind, O. Iron-regulated surface determinants (Isd) of *Staphylococcus aureus*: stealing iron from heme. *Microbes Infect* **6**, 390-397, doi:10.1016/j.micinf.2003.12.008 (2004).

31 Dailey, H. A., Gerdes, S., Dailey, T. A., Burch, J. S. & Phillips, J. D. Noncanonical coproporphyrin-dependent bacterial heme biosynthesis pathway that does not use protoporphyrin. *Proc Natl Acad Sci U S A* **112**, 2210-2215, doi:10.1073/pnas.1416285112 (2015).

32 Lobo, S. A. *et al. Staphylococcus aureus* haem biosynthesis: characterisation of the enzymes involved in final steps of the pathway. *Mol Microbiol* **97**, 472-487, doi:10.1111/mmi.13041 (2015).

33 Mayfield, J. A. *et al.* The chlorite dismutase (HemQ) from *Staphylococcus aureus* has a redox-sensitive heme and is associated with the small colony variant phenotype. *J Biol Chem* **288**, 23488-23504, doi:10.1074/jbc.M112.442335 (2013).

34 Fang, F. C. *Nitric oxide and infection*. (Kluwer Academic/Plenum Publishers, 1999).

35 Guerra, F. E., Borgogna, T. R., Patel, D. M., Sward, E. W. & Voyich, J. M. Epic Immune Battles of History: Neutrophils vs. *Staphylococcus aureus*. *Front Cell Infect Microbiol* **7**, 286, doi:10.3389/fcimb.2017.00286 (2017).

36 Stryjewski, M. E. *et al. Staphylococcus Aureus* Bacteremia Among Patients with Health Care-associated Fever. *Am J Med* **122**, 281-U116, doi:10.1016/j.amjmed.2008.09.040 (2009).

37 Ezraty, B., Gennaris, A., Barras, F. & Collet, J. F. Oxidative stress, protein damage and repair in bacteria. *Nat Rev Microbiol* **15**, 385-396, doi:10.1038/nrmicro.2017.26 (2017).

38 Henderson, B., Allan, E. & Coates, A. R. Stress wars: the direct role of host and bacterial molecular chaperones in bacterial infection. *Infect Immun* **74**, 3693-3706, doi:10.1128/IAI.01882-05 (2006).

39 Singh, V. K. *et al.* Role for dnaK locus in tolerance of multiple stresses in *Staphylococcus aureus*. *Microbiology* **153**, 3162-3173, doi:10.1099/mic.0.2007/009506-0 (2007).

40 Calloni, G. *et al.* DnaK Functions as a Central Hub in the *E. coli* Chaperone Network. *Cell Rep* **1**, 251-264, doi:10.1016/j.celrep.2011.12.007 (2012).

41 Liu, C. P., Zhou, Q. M., Fan, D. J. & Zhou, J. M. PPIase domain of trigger factor acts as auxiliary chaperone site to assist the folding of protein substrates bound to the crevice of trigger factor. *Int J Biochem Cell B* **42**, 890-901, doi:10.1016/j.biocel.2010.01.019 (2010).

42 Deuerling, E., Schulze-Specking, A., Tomoyasu, T., Mogk, A. & Bukau, B. Trigger factor and DnaK cooperate in folding of newly synthesized proteins. *Nature* **400**, 693-696, doi:10.1038/23301 (1999).

43 Keogh, R. A., Zapf, R. L., Wiemels, R. E., Wittekind, M. A. & Carroll, R. K. The Intracellular Cyclophilin PpiB Contributes to the Virulence of *Staphylococcus aureus* Independently of Its Peptidyl-Prolyl cis/trans Isomerase Activity. *Infect Immun* **86**, doi:10.1128/IAI.00379-18 (2018).

44 Sasaki, S. *et al.* Protective role of nitric oxide in *Staphylococcus aureus* infection in mice. *Infection and Immunity* **66**, 1017-1022, doi:Doi 10.1128/Iai.66.3.1017-1022.1998 (1998).

45 Vitko, N. P., Spahich, N. A. & Richardson, A. R. Glycolytic Dependency of High-Level Nitric Oxide Resistance and Virulence in *Staphylococcus aureus*. *Mbio* **6**, doi:ARTN e00045-15
10.1128/mBio.00045-15 (2015).

46 Richardson, A. R., Libby, S. J. & Fang, F. C. A nitric oxide-inducible lactate dehydrogenase enables *Staphylococcus aureus* to resist innate immunity. *Science* **319**, 1672-1676, doi:10.1126/science.1155207 (2008).

47 Brown, G. C., McBride, A. G., Fox, E. J., McNaught, K. S. & Borutaite, V. Nitric oxide and oxygen metabolism. *Biochem Soc T* **25**, 901-904, doi:DOI 10.1042/bst0250901 (1997).

48 Heim, C. E. *et al.* Lactate production by *Staphylococcus aureus* biofilm inhibits HDAC11 to reprogramme the host immune response during persistent infection. *Nat Microbiol*, doi:10.1038/s41564-020-0756-3 (2020).

49 Ibarra, J. A., Perez-Rueda, E., Carroll, R. K. & Shaw, L. N. Global analysis of transcriptional regulators in *Staphylococcus aureus*. *Bmc Genomics* **14**, doi:Artn 126
10.1186/1471-2164-14-126 (2013).

50 Jenul, C. & Horswill, A. R. Regulation of *Staphylococcus aureus* Virulence. *Microbiol Spectr* **6**, doi:10.1128/microbiolspec.GPP3-0031-2018 (2018).
51 Somerville, G. A. & Proctor, R. A. At the Crossroads of Bacterial Metabolism and Virulence Factor Synthesis in Staphylococci. *Microbiol Mol Biol R* **73**, 233-248, doi:10.1128/Mmbr.00005-09 (2009).
52 Majerczyk, C. D. *et al.* *Staphylococcus aureus* CodY negatively regulates virulence gene expression. *Journal of Bacteriology* **190**, 2257-2265, doi:10.1128/Jb.01545-07 (2008).
53 Waters, N. R. *et al.* A spectrum of CodY activities drives metabolic reorganization and virulence gene expression in *Staphylococcus aureus*. *Molecular Microbiology* **101**, 495-514, doi:10.1111/mmi.13404 (2016).
54 Kaiser, J. C. *et al.* Repression of branched-chain amino acid synthesis in *Staphylococcus aureus* is mediated by isoleucine via CodY, and by a leucine-rich. *Plos Genet* **14**, doi:ARTN e1007159
10.1371/journal.pgen.1007159 (2018).
55 Pohl, K. *et al.* CodY in *Staphylococcus aureus*: a Regulatory Link between Metabolism and Virulence Gene Expression. *Journal of Bacteriology* **191**, 2953-2963, doi:10.1128/Jb.01492-08 (2009).
56 Han, A. R. *et al.* The structure of the pleiotropic transcription regulator CodY provides insight into its GTP-sensing mechanism. *Nucleic Acids Res* **44**, 9483-9493, doi:10.1093/nar/gkw775 (2016).
57 Chavakis, T., Wiechmann, K., Preissner, K. T. & Herrmann, M. *Staphylococcus aureus* interactions with the endothelium: the role of bacterial "secretable expanded repertoire adhesive molecules" (SERAM) in disturbing host defense systems. *Thromb Haemost* **94**, 278-285, doi:10.1160/TH05-05-0306 (2005).
58 Hussain, M. *et al.* Identification and characterization of a novel 38.5-kilodalton cell surface protein of *Staphylococcus aureus* with extended-spectrum binding activity for extracellular matrix and plasma proteins. *J Bacteriol* **183**, 6778-6786, doi:10.1128/JB.183.23.6778-6786.2001 (2001).
59 Geraci, J. *et al.* The *Staphylococcus aureus* extracellular matrix protein (Emp) has a fibrous structure and binds to different extracellular matrices. *Sci Rep* **7**, 13665, doi:10.1038/s41598-017-14168-4 (2017).
60 Harraghy, N. *et al.* The adhesive and immunomodulating properties of the multifunctional *Staphylococcus aureus* protein Eap. *Microbiology* **149**, 2701-2707, doi:10.1099/mic.0.26465-0 (2003).
61 Cheng, A. G. *et al.* Genetic requirements for *Staphylococcus aureus* abscess formation and persistence in host tissues. *Faseb Journal* **23**, 3393-3404, doi:10.1096/fj.09-135467 (2009).
62 Rollins, T. E. & Springer, M. S. Identification of the polymorphonuclear leukocyte C5a receptor. *J Biol Chem* **260**, 7157-7160 (1985).
63 Le, Y., Murphy, P. M. & Wang, J. M. Formyl-peptide receptors revisited. *Trends Immunol* **23**, 541-548, doi:10.1016/s1471-4906(02)02316-5 (2002).
64 Teng, T.-S., Ji, A.-l., Ji, X.-Y. & Li, Y.-Z. Neutrophils and immunity: from bactericidal action to being conquered. *Journal of immunology research* **2017** (2017).
65 Postma, B. *et al.* Chemotaxis inhibitory protein of *Staphylococcus aureus* binds specifically to the C5a and formylated peptide receptor. *J Immunol* **172**, 6994-7001, doi:10.4049/jimmunol.172.11.6994 (2004).

66 Prat, C., Bestebroer, J., de Haas, C. J., van Strijp, J. A. & van Kessel, K. P. A new staphylococcal anti-inflammatory protein that antagonizes the formyl peptide receptor-like 1. *J Immunol* **177**, 8017-8026, doi:10.4049/jimmunol.177.11.8017 (2006).

67 Reyes-Robles, T. & Torres, V. J. *Staphylococcus aureus* Pore-Forming Toxins. *Curr Top Microbiol Immunol* **409**, 121-144, doi:10.1007/82_2016_16 (2017).

68 Dumont, A. L. *et al.* Characterization of a new cytotoxin that contributes to *Staphylococcus aureus* pathogenesis. *Mol Microbiol* **79**, 814-825, doi:10.1111/j.1365-2958.2010.07490.x (2011).

69 Ventura, C. L. *et al.* Identification of a novel *Staphylococcus aureus* two-component leukotoxin using cell surface proteomics. *PLoS One* **5**, e11634, doi:10.1371/journal.pone.0011634 (2010).

70 Liu, Q., Yeo, W. S. & Bae, T. The SaeRS Two-Component System of *Staphylococcus aureus*. *Genes (Basel)* **7**, doi:10.3390/genes7100081 (2016).

71 Geiger, T., Goerke, C., Mainiero, M., Kraus, D. & Wolz, C. The virulence regulator Sae of *Staphylococcus aureus*: promoter activities and response to phagocytosis-related signals. *J Bacteriol* **190**, 3419-3428, doi:10.1128/JB.01927-07 (2008).

72 Cho, H. *et al.* Calprotectin Increases the Activity of the SaeRS Two Component System and Murine Mortality during *Staphylococcus aureus* Infections. *PLoS Pathog* **11**, e1005026, doi:10.1371/journal.ppat.1005026 (2015).

73 Kim, M. H. *et al.* Neutrophil survival and c-kit(+)-progenitor proliferation in Staphylococcus aureus-infected skin wounds promote resolution. *Blood* **117**, 3343-3352, doi:10.1182/blood-2010-07-296970 (2011).

74 Spinardi, J. R. *et al. Enterococcus spp.* and *S. aureus* colonization in neutropenic febrile children with cancer. *Germs* **7**, 61-72, doi:10.18683/germs.2017.1110 (2017).

75 Verdrengh, M. & Tarkowski, A. Role of neutrophils in experimental septicemia and septic arthritis induced by *Staphylococcus aureus*. *Infect Immun* **65**, 2517-2521 (1997).

76 Thammavongsa, V., Missiakas, D. M. & Schneewind, O. *Staphylococcus aureus* degrades neutrophil extracellular traps to promote immune cell death. *Science* **342**, 863-866, doi:10.1126/science.1242255 (2013).

77 Jablonski, K. A. *et al.* Novel Markers to Delineate Murine M1 and M2 Macrophages. *PLoS One* **10**, e0145342, doi:10.1371/journal.pone.0145342 (2015).

78 Raes, G. *et al.* FIZZ1 and Ym as tools to discriminate between differentially activated macrophages. *Dev Immunol* **9**, 151-159, doi:10.1080/1044667031000137629 (2002).

79 El Kasmi, K. C. *et al.* Toll-like receptor-induced arginase 1 in macrophages thwarts effective immunity against intracellular pathogens. *Nat Immunol* **9**, 1399-1406, doi:10.1038/ni.1671 (2008).

80 Thurlow, L. R., Joshi, G. S. & Richardson, A. R. Peroxisome Proliferator-Activated Receptor gamma Is Essential for the Resolution of *Staphylococcus aureus* Skin Infections. *Cell Host Microbe* **24**, 261-270 e264, doi:10.1016/j.chom.2018.07.001 (2018).

81 Thurlow, L. R. *et al.* Functional modularity of the arginine catabolic mobile element contributes to the success of USA300 methicillin-resistant *Staphylococcus aureus*. *Cell Host Microbe* **13**, 100-107, doi:10.1016/j.chom.2012.11.012 (2013).

82 Skaar, E. P., Humayun, M., Bae, T., DeBord, K. L. & Schneewind, O. Iron-source preference of *Staphylococcus aureus* infections. *Science* **305**, 1626-1628, doi:10.1126/science.1099930 (2004).

83 Torres, V. J., Pishchany, G., Humayun, M., Schneewind, O. & Skaar, E. P. *Staphylococcus aureus* IsdB is a hemoglobin receptor required for heme iron utilization. *J Bacteriol* **188**, 8421-8429, doi:10.1128/JB.01335-06 (2006).

84 Mikkelsen, J. H., Runager, K. & Andersen, C. B. F. The human protein haptoglobin inhibits IsdH-mediated heme-sequestering by *Staphylococcus aureus*. *J Biol Chem* **295**, 1781-1791, doi:10.1074/jbc.RA119.011612 (2020).

85 Burmester, T., Gerlach, F. & Hankeln, T. Regulation and role of neuroglobin and cytoglobin under hypoxia. *Adv Exp Med Biol* **618**, 169-180, doi:10.1007/978-0-387-75434-5_13 (2007).

86 Gardner, P. R. *et al.* Hemoglobins dioxygenate nitric oxide with high fidelity. *J Inorg Biochem* **100**, 542-550, doi:10.1016/j.jinorgbio.2005.12.012 (2006).

87 Gardner, A. M., Cook, M. R. & Gardner, P. R. Nitric-oxide dioxygenase function of human cytoglobin with cellular reductants and in rat hepatocytes. *J Biol Chem* **285**, 23850-23857, doi:10.1074/jbc.M110.132340 (2010).

88 Xu, R. *et al.* Cytoglobin overexpression protects against damage-induced fibrosis. *Mol Ther* **13**, 1093-1100, doi:10.1016/j.ymthe.2005.11.027 (2006).

89 Amir, R. E., Iwai, K. & Ciechanover, A. The NEDD8 pathway is essential for SCF(beta -TrCP)-mediated ubiquitination and processing of the NF-kappa B precursor p105. *J Biol Chem* **277**, 23253-23259, doi:10.1074/jbc.M200967200 (2002).

90 Ehrentraut, S. F. *et al.* Central role for endothelial human deneddylase-1/SENP8 in fine-tuning the vascular inflammatory response. *J Immunol* **190**, 392-400, doi:10.4049/jimmunol.1202041 (2013).

91 Sufan, R. I. & Ohh, M. Role of the NEDD8 modification of Cul2 in the sequential activation of ECV complex. *Neoplasia* **8**, 956-963, doi:10.1593/neo.06520 (2006).

92 Curtis, V. F. *et al.* Stabilization of HIF through inhibition of Cullin-2 neddylation is protective in mucosal inflammatory responses. *FASEB J* **29**, 208-215, doi:10.1096/fj.14-259663 (2015).

93 Bonita, D. P., Miyake, S., Lupher, M. L., Jr., Langdon, W. Y. & Band, H. Phosphotyrosine binding domain-dependent upregulation of the platelet-derived growth factor receptor alpha signaling cascade by transforming mutants of Cbl: implications for Cbl's function and oncogenicity. *Mol Cell Biol* **17**, 4597-4610, doi:10.1128/mcb.17.8.4597 (1997).

94 Levkowitz, G. *et al.* c-Cbl/Sli-1 regulates endocytic sorting and ubiquitination of the epidermal growth factor receptor. *Genes Dev* **12**, 3663-3674, doi:10.1101/gad.12.23.3663 (1998).

95 Palazon-Riquelme, P. *et al.* USP7 and USP47 deubiquitinases regulate NLRP3 inflammasome activation. *EMBO Rep* **19**, doi:10.15252/embr.201744766 (2018).

96 Chui, A. J. *et al.* N-terminal degradation activates the NLRP1B inflammasome. *Science* **364**, 82-85, doi:10.1126/science.aau1208 (2019).

97 Sandstrom, A. *et al.* Functional degradation: A mechanism of NLRP1 inflammasome activation by diverse pathogen enzymes. *Science* **364**, doi:10.1126/science.aau1330 (2019).

98 Nazio, F. *et al.* mTOR inhibits autophagy by controlling ULK1 ubiquitylation, self-association and function through AMBRA1 and TRAF6. *Nat Cell Biol* **15**, 406-416, doi:10.1038/ncb2708 (2013).

99 Shi, C. S. & Kehrl, J. H. TRAF6 and A20 regulate lysine 63-linked ubiquitination of Beclin-1 to control TLR4-induced autophagy. *Sci Signal* **3**, ra42, doi:10.1126/scisignal.2000751 (2010).

100 Roy, C. *et al.* The topoisomerase II inhibitor teniposide (VM-26) induces apoptosis in unstimulated mature murine lymphocytes. *Exp Cell Res* **200**, 416-424, doi:10.1016/0014-4827(92)90190-j (1992).

101 Delic, J., Morange, M. & Magdelenat, H. Ubiquitin pathway involvement in human lymphocyte gamma-irradiation-induced apoptosis. *Mol Cell Biol* **13**, 4875-4883, doi:10.1128/mcb.13.8.4875 (1993).

102 Liu, J., Furukawa, M., Matsumoto, T. & Xiong, Y. NEDD8 modification of CUL1 dissociates p120(CAND1), an inhibitor of CUL1-SKP1 binding and SCF ligases. *Mol Cell* **10**, 1511-1518, doi:10.1016/s1097-2765(02)00783-9 (2002).

103 Kamitani, T., Kito, K., Fukuda-Kamitani, T. & Yeh, E. T. Targeting of NEDD8 and its conjugates for proteasomal degradation by NUB1. *J Biol Chem* **276**, 46655-46660, doi:10.1074/jbc.M108636200 (2001).

104 Kito, K., Yeh, E. T. & Kamitani, T. NUB1, a NEDD8-interacting protein, is induced by interferon and down-regulates the NEDD8 expression. *J Biol Chem* **276**, 20603-20609, doi:10.1074/jbc.M100920200 (2001).

105 Jassal, B. *et al.* The reactome pathway knowledgebase. *Nucleic Acids Res* **48**, D498-D503, doi:10.1093/nar/gkz1031 (2020).

106 Gutierrez, D. B. *et al.* An Integrated, High-Throughput Strategy for Multiomic Systems Level Analysis. *J Proteome Res* **17**, 3396-3408, doi:10.1021/acs.jproteome.8b00302 (2018).

107 James C. Pino, A. L. R. L., Leonard A. Harris, Danielle B. Gutierrez, Melissa A. Farrow, Nicole Muszynski, Tina Tsui, Jeremy L. Norris, Richard M. Caprioli, John P. Wikswo, Carlos F. Lopez. A computational framework to explore cellular response mechanisms from multi-omics datasets. doi:https://doi.org/10.1101/2020.03.02.974121 (2020).

108 Benesch, R. & Benesch, R. E. The effect of organic phosphates from the human erythrocyte on the allosteric properties of hemoglobin. *Biochem Biophys Res Commun* **26**, 162-167, doi:10.1016/0006-291x(67)90228-8 (1967).

109 Benesch, R., Benesch, R. E. & Yu, C. I. Reciprocal binding of oxygen and diphosphoglycerate by human hemoglobin. *Proc Natl Acad Sci U S A* **59**, 526-532, doi:10.1073/pnas.59.2.526 (1968).

110 O'Neill, L. A. & Pearce, E. J. Immunometabolism governs dendritic cell and macrophage function. *J Exp Med* **213**, 15-23, doi:10.1084/jem.20151570 (2016).

111 Silva-Garcia, O. *et al.* Glycogen Synthase Kinase 3alpha Is the Main Isoform That Regulates the Transcription Factors Nuclear Factor-Kappa B and cAMP Response Element Binding in Bovine Endothelial Cells Infected with *Staphylococcus aureus*. *Front Immunol* **9**, 92, doi:10.3389/fimmu.2018.00092 (2018).

112 Powers-Greenwood, S. L., Rahmatullah, M., Radke, G. A. & Roche, T. E. Separation of protein X from the dihydrolipoyl transacetylase component of the mammalian pyruvate dehydrogenase complex and function of protein X. *J Biol Chem* **264**, 3655-3657 (1989).

113 Lawson, J. E., Behal, R. H. & Reed, L. J. Disruption and mutagenesis of the Saccharomyces cerevisiae *PDX1* gene encoding the protein X component of the pyruvate dehydrogenase complex. *Biochemistry* **30**, 2834-2839, doi:10.1021/bi00225a015 (1991).

114 Liu, X. *et al.* Acetate Production from Glucose and Coupling to Mitochondrial Metabolism in Mammals. *Cell* **175**, 502-513 e513, doi:10.1016/j.cell.2018.08.040 (2018).
115 Houten, S. M. & Wanders, R. J. A general introduction to the biochemistry of mitochondrial fatty acid beta-oxidation. *J Inherit Metab Dis* **33**, 469-477, doi:10.1007/s10545-010-9061-2 (2010).
116 Yang, C. *et al.* Glutamine oxidation maintains the TCA cycle and cell survival during impaired mitochondrial pyruvate transport. *Mol Cell* **56**, 414-424, doi:10.1016/j.molcel.2014.09.025 (2014).
117 Tillander, V., Alexson, S. E. H. & Cohen, D. E. Deactivating Fatty Acids: Acyl-CoA Thioesterase-Mediated Control of Lipid Metabolism. *Trends Endocrinol Metab* **28**, 473-484, doi:10.1016/j.tem.2017.03.001 (2017).
118 Cox, J. & Mann, M. MaxQuant enables high peptide identification rates, individualized p.p.b.-range mass accuracies and proteome-wide protein quantification. *Nat Biotechnol* **26**, 1367-1372, doi:10.1038/nbt.1511 (2008).
119 Bateman, A. *et al.* UniProt: a worldwide hub of protein knowledge. *Nucleic Acids Res* **47**, D506-D515, doi:10.1093/nar/gky1049 (2019).
120 Perez-Riverol, Y. *et al.* The PRIDE database and related tools and resources in 2019: improving support for quantification data. *Nucleic Acids Res* **47**, D442-D450, doi:10.1093/nar/gky1106 (2019).

Figure Legends:

Figure 1: microLESA sampling strategy and results.

A) Schematic of regions selected for collection shown using autofluorescence and H&E.

B) Overview of bacterial and host proteins identified at different timepoints and across different regions within infected renal tissue. Total host proteins: 2399. Total bacterial proteins: 31.

Figure 2: Overview of *S. aureus* proteins identified in the different abscess regions. Staphylococcal proteins were found in the interface and SAC of renal abscesses at 4 or 10 dpi. Red circles denote proteins that were present at the specific timepoint/region, while grey circles depict the absence of a specific protein. General functional categories for proteins and protein groups are shown. Further information concerning proteins in this list can be found in Table S2. 0816: SAUSA300_0816; 1656: SAUSA300_1656.

Figure 3: Comparison of the proteome from the different regions in and around staphylococcal tissue abscesses. Data is combined host and bacterial proteins.

A) UpSet plot displaying unique and shared proteins identified from the three sampled locations.

B) Comparison of the proteome from individual regions over the course of infections (4 dpi vs. 10 dpi).

Figure 4: Spatiotemporal distribution of immune cell markers, hemoglobin components, NEDDylation-associated factors in infected tissue. Host immune proteins were found in the interface and SAC of renal abscessess at 4 and 10 dpi. Blue circles denote proteins that were present at the specified timepoint/region, while grey circles depict the absence of a specific protein.

Figure 5: Overview of spatiotemporal distribution of proteins involved in central metabolism. Arrows denote metabolic pathways, ovals indicate genes, and colors indicate time point and region where proteins were detected.

Figure S1: Examples of microLESA from different regions. Locations of microLESA sampling (colored dots) are shown on autofluorescence images of infected kidneys (10 dpi). Regions are shown by color-coded circles.

Figure S2: Spatiotemporal distribution of metabolic proteins during infection. Blue circles denote proteins that were present at the specified timepoint/region, while grey circles depict the absence of a specific protein.

Table S1: List of host-derived proteins found by presence at time point and biological region, including platform used for identification (P = Protalizer, MQ = MaxQuant).

Table S2: List of bacterial proteins detected and their localizations based on stringent search criteria from Protalizer and MaxQuant. No bacterial proteins were detected in the cortex.

Table S3: List of bacterial proteins detected and their localizations with lower identification confidence.

A

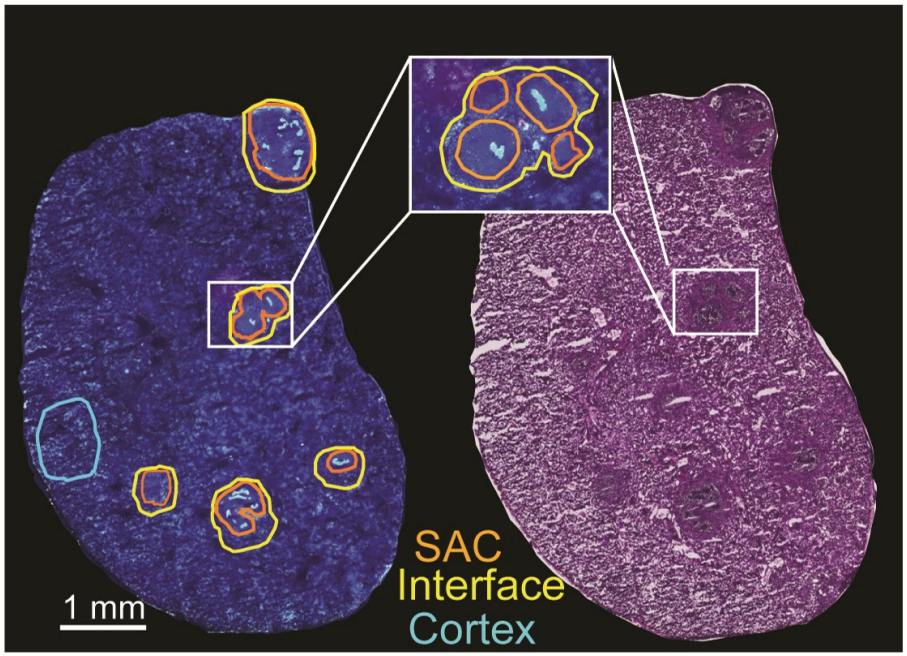
SAC
Interface
Cortex
1 mm

B

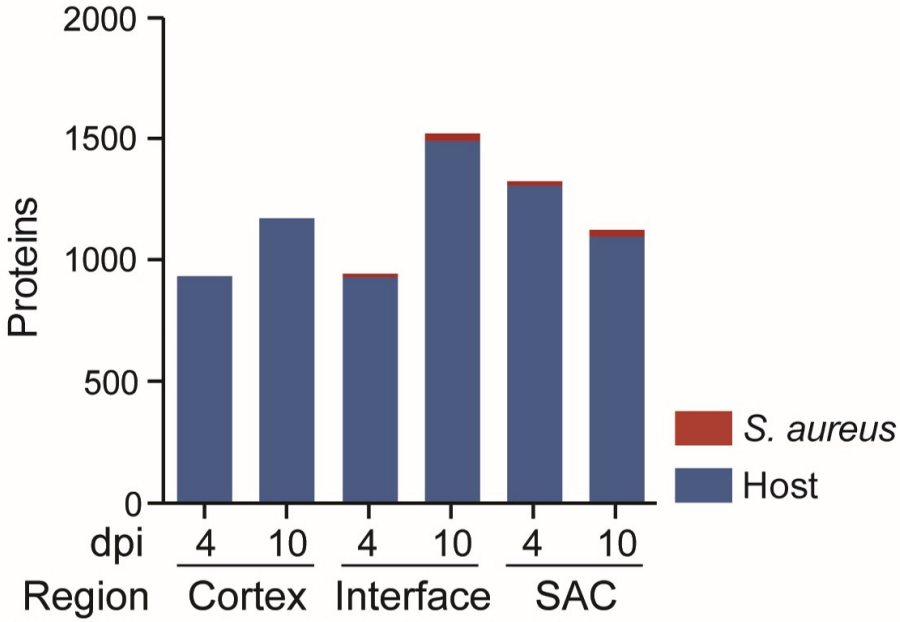
2000
1500
1000
500
0
Proteins
dpi
4
10
4
10
4
10
Region
Cortex
Interface
SAC
S. aureus
Host

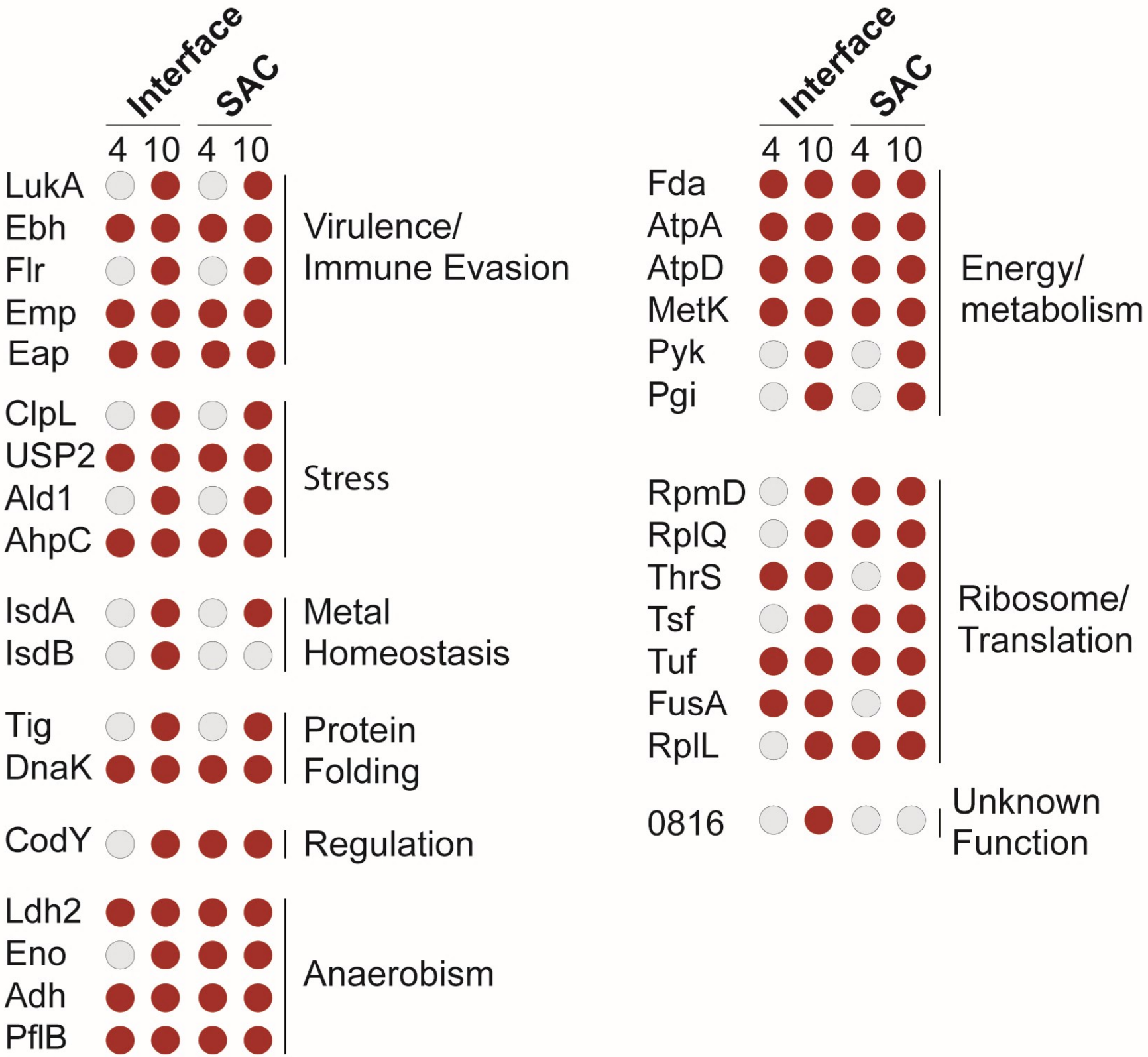
Interface
SAC
4 10 4 10
LukA
Ebh
Flr
Emp
Eap
Virulence/
Immune Evasion
ClpL
USP2
Ald1
AhpC
Stress
IsdA
IsdB
Metal
Homeostasis
Tig
DnaK
Protein
Folding
CodY
Regulation
Ldh2
Eno
Adh
PflB
Anaerobism
Interface
SAC
4 10 4 10
Fda
AtpA
AtpD
MetK
Pyk
Pgi
Energy/
metabolism
RpmD
RplQ
ThrS
Tsf
Tuf
FusA
RplL
Ribosome/
Translation
0816
Unknown
Function

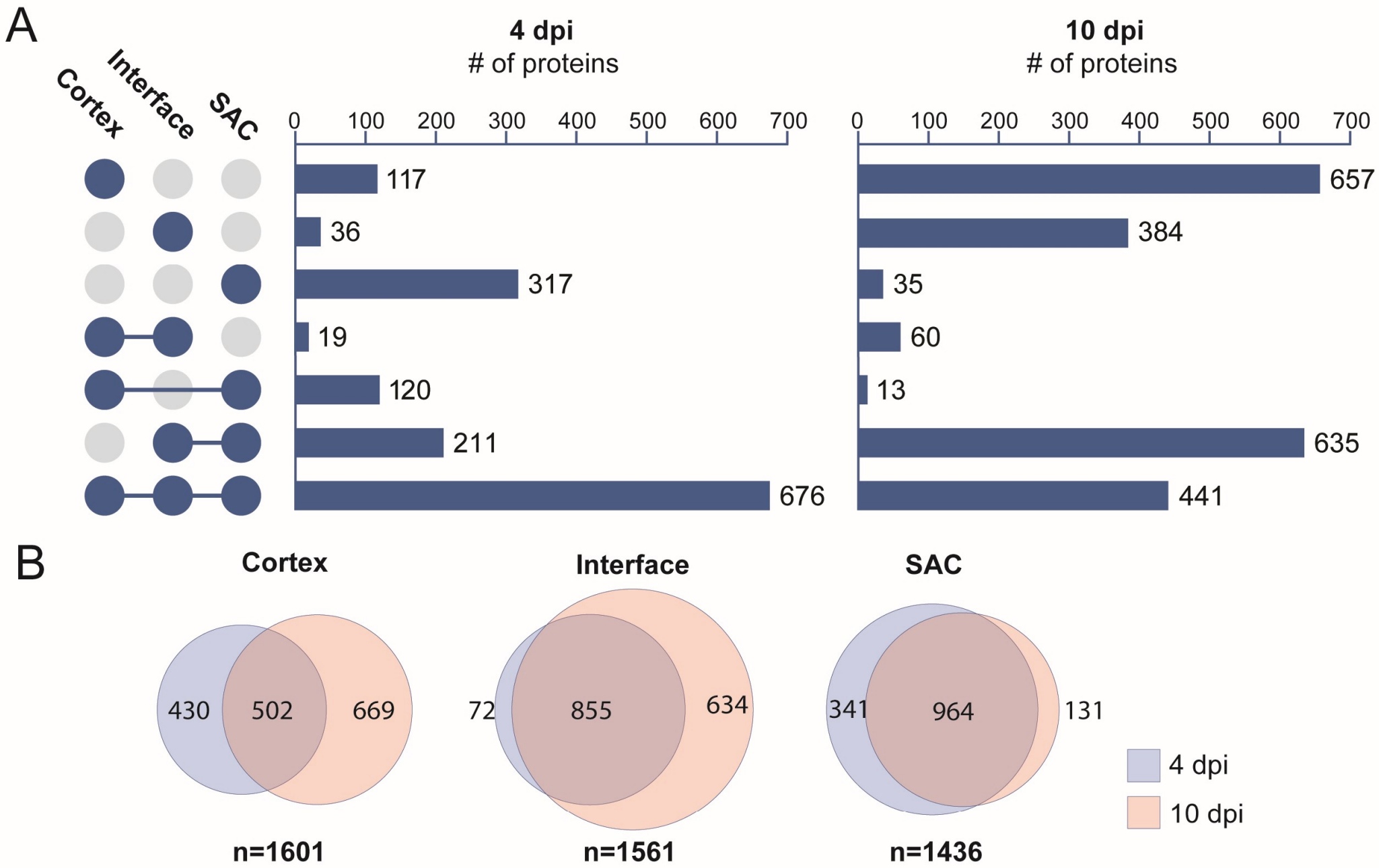
A
Cortex
Interface
SAC
4 dpi
# of proteins
0
100
200
300
400
500
600
700
117
36
317
19
120
211
676
10 dpi
# of proteins
0
100
200
300
400
500
600
700
657
384
35
60
13
635
441
B
Cortex
430
502
669
n=1601
Interface
72
855
634
n=1561
SAC
341
964
131
n=1436
4 dpi
10 dpi

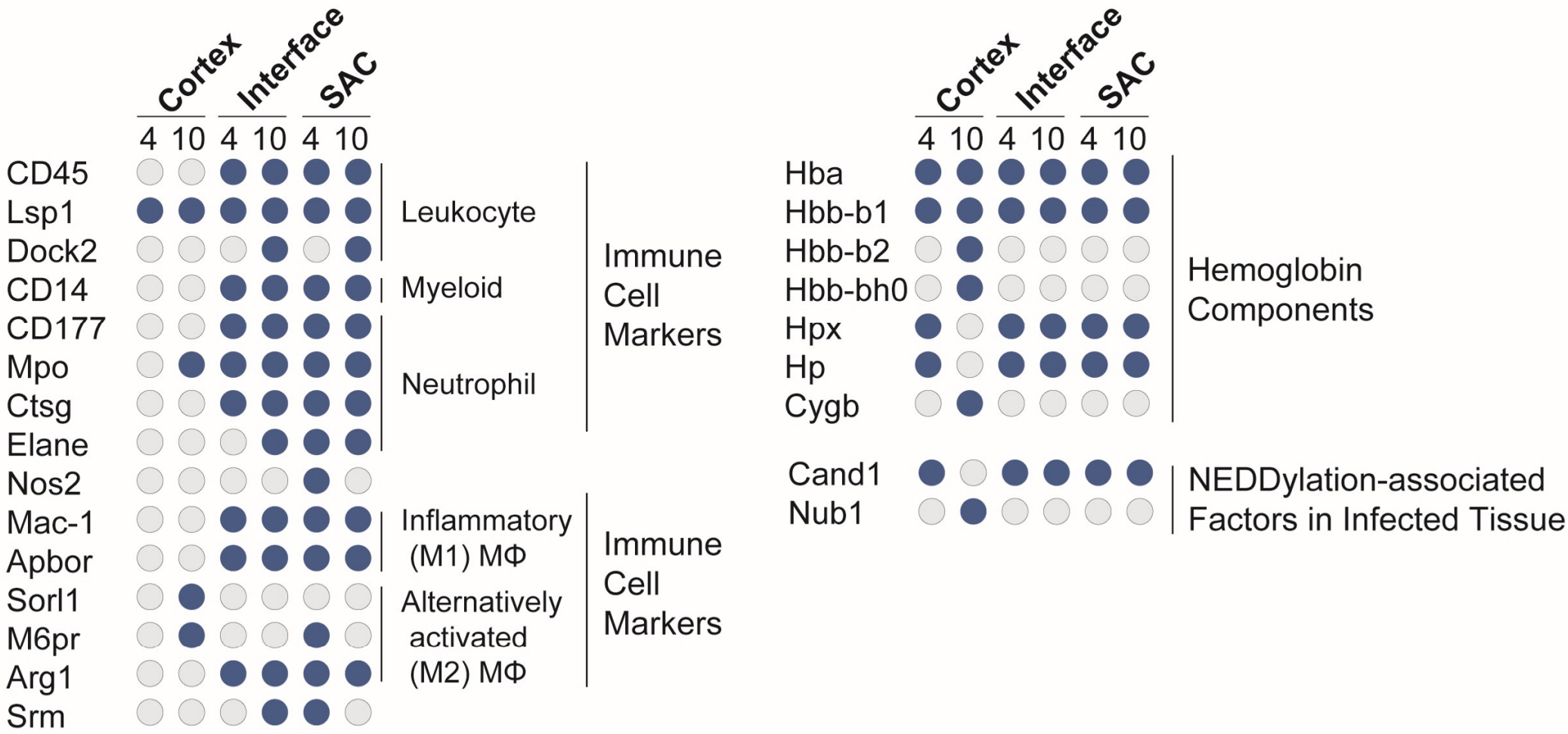
Cortex
Interface
SAC
4 10 4 10 4 10
CD45
Lsp1
Dock2
CD14
CD177
Mpo
Ctsg
Elane
Nos2
Mac-1
Apbor
Sorl1
M6pr
Arg1
Srm
Leukocyte
Myeloid
Neutrophil
Inflammatory (M1) MΦ
Alternatively activated (M2) MΦ
Immune Cell Markers
Immune Cell Markers
Hba
Hbb-b1
Hbb-b2
Hbb-bh0
Hpx
Hp
Cygb
Hemoglobin Components
Cand1
Nub1
NEDDylation-associated Factors in Infected Tissue

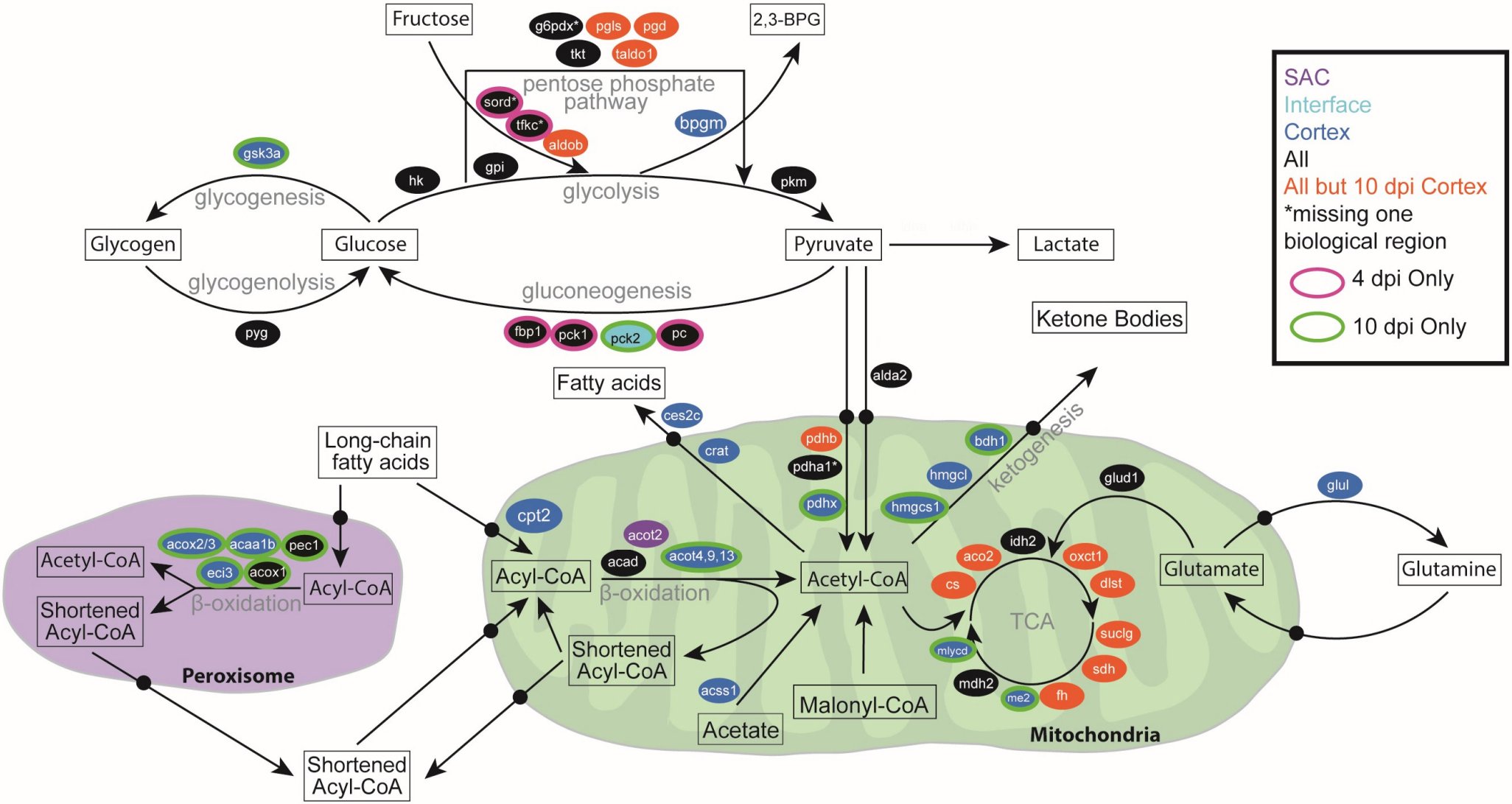
Fructose
g6pdx*
pgls
pgd
tkt
taldo1
2,3-BPG
pentose phosphate pathway
sord*
tfkc*
aldob
bpgm
gsk3a
gpi
hk
glycogenesis
glycolysis
pkm
Glycogen
Glucose
Pyruvate
Lactate
glycogenolysis
gluconeogenesis
pyg
fbp1
pck1
pck2
pc
Ketone Bodies
Fatty acids
alda2
ces2c
crat
Long-chain fatty acids
pdhb
pdha1*
pdhx
bdh1
hmgcl
hmgcs1
ketogenesis
glud1
glul
cpt2
acot2
acad
acot4,9,13
Acyl-CoA
β-oxidation
Acetyl-CoA
idh2
aco2
oxct1
cs
dlst
TCA
suclg
sdh
mdh2
me2
fh
mlycd
Glutamate
Glutamine
Shortened Acyl-CoA
acss1
Acetate
Malonyl-CoA
Mitochondria
acox2/3
acaa1b
pec1
eci3
acox1
Acetyl-CoA
Acyl-CoA
β-oxidation
Shortened Acyl-CoA
Peroxisome
Shortened Acyl-CoA
SAC
Interface
Cortex
All
All but 10 dpi Cortex
*missing one biological region
4 dpi Only
10 dpi Only